Study of binary lead-tin alloys using a new procedure based on calibration-free laser induced breakdown spectroscopy

I. Urbina, D. Carneiro, S. Rocha, E. Farias, F. Bredice, V. Palleschi

PII: S0584-8547(19)30564-6

DOI: https://doi.org/10.1016/j.sab.2020.105902

Reference: SAB 105902

To appear in: *Spectrochimica Acta Part B: Atomic Spectroscopy*

Received date: 13 November 2019

Revised date: 16 June 2020

Accepted date: 16 June 2020

Please cite this article as: I. Urbina, D. Carneiro, S. Rocha, et al., Study of binary lead-tin alloys using a new procedure based on calibration-free laser induced breakdown spectroscopy, *Spectrochimica Acta Part B: Atomic Spectroscopy* (2019), https://doi.org/10.1016/j.sab.2020.105902

Study of binary lead-tin alloys using a new procedure based on calibration-free laser induced breakdown spectroscopy

I. Urbina[1*], D. Carneiro[2,3], S. Rocha[2], E. Farias[2], F. Bredice[1] and V. Palleschi[4]

1. Centro de Investigaciones Ópticas, P.O. Box 3 C. P.1897 Gonnet, La Plata, Argentina.
2. Universidad Federal de Roraima, Boa Vista, Brasil.
3. Centro Universitário Estácio da Amazônia – Boa Vista, Roraima – Brasil.
4. Applied and Laser Spectroscopy Laboratory, Institute of Chemistry of Organometallic Compounds, Research Area of National Research Council, Via G. Moruzzi, 1, 56124 Pisa, Italy.

Abstract

The objective of this work is to present a novel procedure based on the time resolved Boltzmann plot, and the Calibration-free Laser Induced Breakdown Spectroscopy techniques, to determine the composition of the samples by exploiting the temporal evolution of the spectral lines generated in the laser-produced plasma. As an example of the application of this procedure, Laser Induced Breakdown Spectroscopy spectra were acquired on binary lead – tin alloys of different composition at several delay times, from 1 to 4 μs with a step of 0.5 μs after the onset of the plasma. The matrix change of the alloys was studied through the determination of the constants that characterize the temporal evolution of plasma. The effects of self-absorption were also taken into account and compensated. The application of the proposed method allowed us to determine the concentrations of lead (Pb) and tin (Sn) in the alloys with an error lower than 5%.

Keywords: LIBS, Calibration Free LIBS, 3D Boltzmann plot, Temporal evolution, Pb-Sn alloys.

Corresponding author: ivan@ciop.unlp.edu.ar

1. Introduction

The Calibration-Free, (CF), [1] approach to the LIBS quantitative analysis of materials is based on the assumption of local thermodynamics equilibrium, (LTE), [2]. This technique allows quantitative analysis of the samples without the use of reference samples and is not affected by the matrix effect [3]. Since its original formulation, the calibration- free laser induced breakdown spectroscopy (CF-LIBS method has been refined for taking into account self-absorption effects [4] and non-homogeneity of the plasma [5,6].

In order to obtain good results with this procedure, the correct determination of the plasma temperature is very important and, consequently, the selection of the spectral lines to be used in the construction of the Boltzmann plot is a critical factor influencing the analytical accuracy of the method.

In previous works, [7–9] some of the authors showed that it is possible to determine, among other things, the electron temperature of the plasma through the characterization of the dependence of the spectral line intensities in a space of coordinates "ln (I/g_kA_{ik})", "E_k" and "time" (Boltzmann Surface) which E_k is the upper level energy of the single emission line. Where I is the integrated intensity of a spectral line, g_k is the degeneracy of upper level of the transition, with energy E_k and A_{ki} is the transition probability from level k to level i.

In a conventional Boltzmann plot, the experimental values of the intensities of the spectral lines in the LIBS spectrum are represented as discrete points in the plane defined by the coordinates "ln (I/g_kA_{ik})" and "E_k". If the measurement is repeated at different times after the onset of the plasma, each spectrum is associated to an independent Boltzmann plot. One of the advantages of the 3D Boltzmann plot technique, [7–9], on the contrary, is the definition of a smooth surface which represents the dependence of the signal on both the line energy and delay time. Each point of the Boltzmann surface is the result of the simultaneous elaboration of all the lines involved in the analysis.

From the analysis of the Boltzmann surface an expression for the plasma temperature as a function of time can be obtained. The new CF-LIBS procedure presented in this work is based on the use of the function $T = T(t)$ derived from the 3D Boltzmann plot for the CF determination of the composition of the sample under study.

In the traditional CF-LIBS method, the spectral line intensities used in the analysis are determined at a fixed delay time. Then the Boltzmann plot is constructed, the logarithms of the line intensity, divided by the corresponding transition probability and upper level degeneracy are fitted with a linear model as a function of the upper energy of the transition, and the intercepts of the best fit lines (one for each of the species present in the sample) with the y-axis are used for calculating the concentrations of the species.

In the proposed method, on the contrary, the information on the species concentration is obtained for each spectral line and for each instant of time in which the spectrum was recorded. Therefore, a better precision with respect to a classical CF-LIBS approach is expected.

2. Experimental setup and materials

The LIBS system used for the measurements here reported consists of a LIBSpector experimental chamber coupled to an ARYELLE-Butterfly (LaserTechnick Berlin-LTB) spectrometer equipped with an ICCD (iStar Model DH334T-18F-03-27A by Andor), relative resolution $\frac{\lambda}{\Delta\lambda} = 9600$ in the range between 350 and 820 nm, and a Brilliant b Nd:YAG laser from Quantel (France), 5 ns pulse width, with maximum repetition rate of 10 Hz and wavelength of 1064 nm. The spectrometer was calibrated both in wavelength and radiometrically, and during the experiment the temperature and humidity were monitored in order to guarantee the same environmental conditions throughout the whole experiment. Lead-tin (Pb-Sn) alloy samples with the following stochiometric composition were used: 85% Pb-15% Sn, 70% Pb-30% Sn, 30% Pb-70% Sn and 15% Pb-85% Sn. The plasmas were generated at the laser energy of 130 mJ, in air at atmospheric pressure. The laser beam was focused on the target using a 250 mm focal length lens, producing a laser spot of about 0.6 mm in diameter at the sample surface. The plasma radiation was directed to the spectrometer by mirrors and optical fiber. The LIBS spectra where acquired at several delay times, from 1 to 4 μs with a step of 500 ns after the breakdown, with an integration time of 50 ns. Each spectrum corresponded to the accumulation of 30 laser pulses. After each accumulation, the sample was moved to avoid the formation of deep craters.

3. Time-resolved CF-LIBS

The conventional CF-LIBS algorithm assumes the validity of the Boltzmann equation:

$$I_0 = Fn_a g_k A_{ki} \frac{e^{-\frac{E_k}{k_B T}}}{U_a(T)} \qquad (1)$$

Where I_0 is the intensity of a line of the species a, T is the plasma electron temperature, g_k is the degeneracy of upper level of the transition, with energy E_k , A_{ki} is the transition probability from level k to level i, k_B is the Boltzmann constant and $U_a(T)$ is the partition function of the species a at the temperature T. n_a is the number of atoms of the species a and F is a factor taking into account the efficiency of the collection system.

If a consistent part of the light emitted is reabsorbed by the plasma before reaching the detector, the proportionality relation between number density of the species and LIBS intensity expressed by eq. (1) would not hold anymore. Assuming a Lorentzian lineshape, it can be demonstrated [10] that the measured integral intensity of the (self-absorbed) LIBS line I and its full width at half maximum (FWHM) $\Delta\lambda$ would change with respect to the optically thin limits I_0 and $\Delta\lambda_0$ according to the relations:

$$I = SA^{\beta} I_0$$
$$\Delta\lambda = SA^{-\alpha} \Delta\lambda_0 \qquad (2)$$

where α=0.54, β=0.46 and

$$SA = \frac{(1-exp(k(\lambda_0)l))}{k(\lambda_0)l} \quad (3)$$

λ_0 is central wavelength of the line, l is the size of the plasma and $k(\lambda_0)$ is the absorption coefficient defined as:

$$k(\lambda_0) = \frac{\lambda_0^4}{8\pi c} A_{ki} g_i \frac{exp\left(-E_i/KT\right)}{U(T)} \frac{1}{\Delta\lambda_0} \quad (4)$$

where c is the speed of light, g_i is the degeneracy and E_i is lower energy level of the considered transition.

The relationship between the integrated intensity of a self-absorbed line I with its optically thin limit I_0 can be written as [4]:

$$I_0 = \left(\frac{\Delta\lambda}{\Delta\lambda_0}\right)^{\beta/\alpha} I \quad (5)$$

The intensities of all the spectra lines used in this work (see Table I) were corrected according to Eq. (5) for compensating the effect of self-absorption.

Table I: Spectral lines used in this work.

Specie	λ (nm)	ω_s (10^{-17} nm/cm^3)	A_{kj} x 10^7 (s^{-1})	g_i	E_i (cm^{-1})	g_k	E_k (cm^{-1})
Pb I	363.95	0.0153 [11]	3.2 [12]	3	7819.3	3	35287.2
Pb I	368.34	0.0131 [11]	13.7 [12]	3	7819.3	1	34959.9
Pb I	373.99	0.0112 [13]	7.3 [12]	5	21457.8	5	48188.6
Pb II	424.49	0.19 [14]	-	6	68964.3	8	92515.2
Pb II	438.65	0.13 [15]	14.71 [16]	4	68739.6	6	92530.7
Pb I	500.54	0.0075 [11]	2.7 [12]	1	29446.8	3	49439.6
Pb II	537.23	0.227 [15]	-	-	-		-
Pb II	560.89	0.14 [14]	12.45 [17]	2	59448.6	4	77272.6
Pb II	666.02	0.12 [14]	7.38 [17]	2	59448.6	2	74459.0
Sn I	380.10	0.045 [18]	3.689 [19]	5	8613.0	3	34914.3
Sn I	452.47	0.286 [11]	1.366 [19]	1	17162.5	3	39257.1
Sn II	645.35	0.29 [11]	7.0 [12]	2	56886.4	4	72377.4

3.1 Conventional calibration free approach

Briefly, the principle of the CF-LIBS technique is based on the determination of the intercept q_a between the linear fit of the points in the Boltzmann plot and the y axis defined as:

$$y = \ln\left(\frac{I(T)}{g_k A_{kj}}\right) \quad (6)$$

According to the expression for the Boltzmann plot:

$$ln\left(\frac{I(T)}{g_k A_{kj}}\right) = -\frac{E}{kT} + ln\left(\frac{Fn_a}{U_a(T)}\right) \quad (7)$$

$$\therefore q_a(T) = ln\left(\frac{Fn_a}{U_a(T)}\right) \quad (8)$$

$q_a(T)$ is a function of the number of atoms N_a of the individual species a in the plasma, $U_a(T)$ is the value of the partition function of the species a at the temperature T and F is an unknown parameter which accounts for the instrumental response of the system.
The number density of each species can be thus derived from Eq. (8)

$$n_a = \frac{e^{q_a(T)}U_a(T)}{F} \Rightarrow C_a = \frac{n_a}{\sum_i n_i} \quad (9)$$

To calculate the total number density of the element of interest is necessary to apply this procedure over the neutral and the ionization states of the species which are present with significant abundance in the plasma.

3.2 3D Calibration Free LIBS

The Boltzmann equation (eq. 1) links the intensity of the line measured at time a time t with the plasma temperature at that time and the numerical concentration of the species $n_a(t)$. Contrarily to the elemental number concentration N_a, which does not vary during the evolution of the plasma, the species concentrations change in time. This is due to the changes in the equilibrium between neutral atoms and ions in the plasma, which is given by the Saha-Eggert equation:

$$\frac{n_a^{II}(t)}{n_a^{I}(t)} = \frac{2}{n_e(t)}\Lambda(\mathrm{t})^{-3}\frac{U^{II}(T(t))}{U^{I}(T(t))}e^{-E_{ion}/k_BT(t)} \quad (10)$$

with $n_a^I(t) + n_a^{II}(t) = N_a$.
Λ is the thermal wavelength of the electron:

$$\Lambda(\mathrm{t}) = \sqrt{\frac{2\pi\hbar^2}{m_e k_B T(t)}} \quad (11)$$

where m_e is the electron mass and $\hbar$ is the reduced Planck constant. The time evolution of the line intensity in eq. (1) thus depends in a very complex way on the plasma temperature (and the electron number density). The full expression is derived in Appendix A.
However, if the numerical concentration of one of the species is predominant with respect to the other, we can assume that the intensity of the lines corresponding to this species would depend on $n_a(t) \cong N_a$ (with $n_a(t)$ representing either $n_a^{II}(t)$ or $n_a^{I}(t)$, according to which species is dominant for that element).
Therefore, if the approximation is justified, in eq. (8) the variation in time of the product Fn_a could be neglected.
In this work we will take T_0 as the temperature corresponding to the shorter time delay used in our experiment (that is, 1 microsecond after the laser pulse).

We will thus set this time as the origin of the time scale, at $t_0 = 0$. Substituting the expression of $q_a(T)$ from eq. (8), we obtain:

$$q_a(T_0) - q_a(T) = ln\left(\frac{U_a(T)}{U_a(T_0)}\right) \quad (12)$$

$$q_a(T_0) = ln\left(\frac{I(T)}{g_k A_{kj}}\right) + \frac{E}{kT} + ln\left(\frac{U_a(T)}{U_a(T_0)}\right) \quad (13)$$

To the determination of $q_a(T_0)$ concur NxM experimental values, where N is the number of lines used and M is the number of acquired spectra.

According to the 3D Boltzmann plot method [20], the temporal evolution of the intensity of a line n can be expressed as

$$ln\left(\frac{I_n(t)}{I_n(t_0)}\right) = \sum_{i=1}^{S} b_i^n t^i \quad (14)$$

Considering eq. (1), we also have that

$$ln\left(\frac{I_n(t)}{I_n(t_0)}\right) = \sum_{i=1}^{S} (B_i E_k^n + \delta_i)\ t^i \quad (15)$$

with

$$ln\left(\frac{U(T_0)}{U(T)}\right) = \sum_{i=1}^{S} \delta_i t^i \quad (16)$$

The b_i^n coefficients depend linearly on the upper level energy of the transition E_k^n; therefore, a new set of parameters B_i can be calculated as the slope of the plot of the b_i vs. the energy of the upper level of the transition:

$$b_i^n = B_i E_k^n + \delta_i \quad (17)$$

For all the spectral lines studied in this work it was sufficient to use a single term in eq. (14), then

$$ln\left(\frac{I_n(t)}{I_n(t_0)}\right) = b_1^n t \quad (18)$$

and

$$ln\left(\frac{U(T_0)}{U(T)}\right) = \delta_1 t \quad (19)$$

4. Experimental results

The evaluation of the electron number density of the LIBS plasma, at the different delays is crucial for assessing the validity of the approximation of having the numerical concentration of one species predominant with respect to the other. In our case, we have a binary lead-tin, (Pb-Sn) alloy; the approximation should thus be valid for both the elements (although it's not necessary that the same species, neutral or ionic, would be predominant for the two elements).

The electron number density was obtained through the measurement of the Stark broadening of the hydrogen Balmer α line at 656.28 nm. The results do not rely on the fulfilment of the LTE conditions [21]. They are shown in Figure 1.

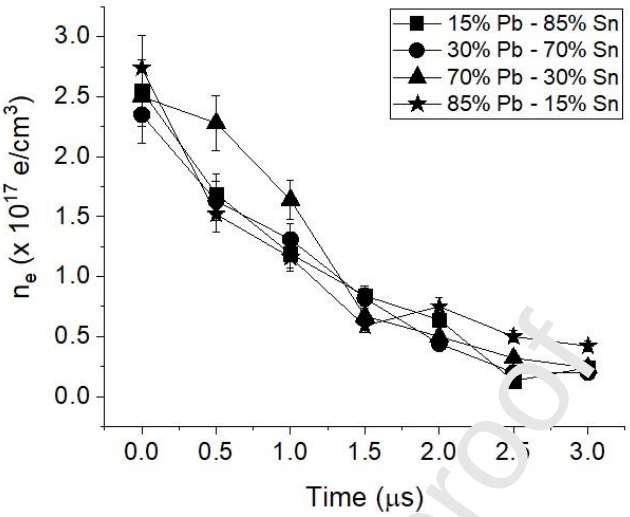

Figure 1 – Time evolution of the electron number density for the four samples considered. The error bars correspond to the uncertainty caused by the precision in the measurement of the width of the line H alpha.

The electron number density is comprised between about 2.5 x 10^{17} e/cm^3 and 0.5 x 10^{17} e/cm^3. Considering that the typical plasma temperatures in the time interval under study would be around 1eV, we can estimate a ratio between ions and neutral atoms larger than 9 for Pb and 7 for Sn at delay times shorter than 2.5 μs. Therefore, except for the late stage of plasma evolution, the ionic species can be considered as predominant with respect to the neutrals.

We have four reliable ionic lines for Pb, but only one for Sn. This would not prevent the calculation of the δ_1^{Sn} , since it can be determined directly from eq. (17) once the parameter B_1 is known from the temporal analysis of the Pb lines.

In figure 2 the b_i vs. E_k plots are shown, for Pb in the four samples.

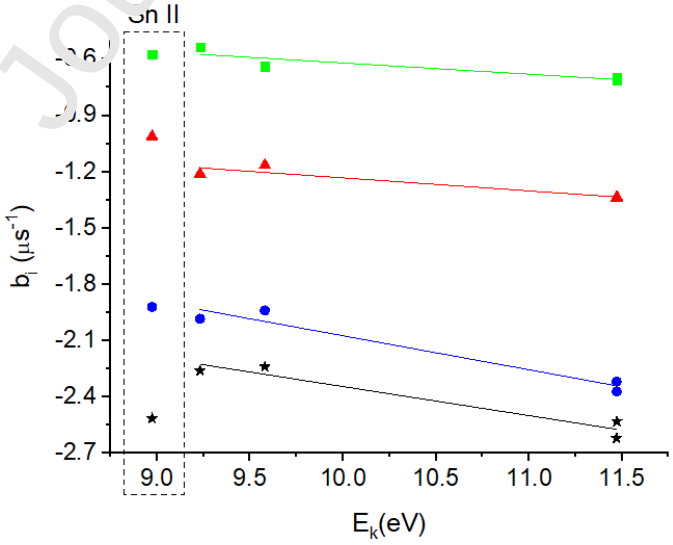

Figure 2 – The b_i coefficients, plotted as a function of the upper energy of the level of the transition. The points at 9 eV corresponds to the Sn II line. (Square) 15%Pb-85%Sn, (circle) 30%Pb-70%Sn, (triangle) 70%Pb-30%Sn, (star) 85%Pb-15%Sn.

The values of B_1, δ_1^{Pb}, and δ_1^{Sn} are reported in Table II, along with the value of the electron temperature for the four samples at t=0 (1 μs in our case), obtained by conventional Saha-Boltzmann plot [22].

Table II- Parameters of the 3D-Boltzmann plot for the samples considered. The error correspond to the standard deviation in the calculation of these coefficients

	T_0 (eV)	B_1 (μs^{-1}/eV)	δ_1^{Pb} (μs^{-1})	δ_1^{Sn} (μs^{-1})	q_{PbII}	q_{SnII}
Pb85-Sn15	1.18±0.04	-0.15±0.03	-0.8±0.3	-1.2±0.3	21.77±0.07	19.25±0.04
Pb70-Sn30	1.08±0.04	-0.07±0.02	-0.5±0.2	-0.4±0.2	22.10±0.03	20.78±0.02
Pb30-Sn70	1.17±0.04	-0.18±0.03	-0.3±0.3	-0.3±0.3	21.28±0.08	21.57±0.04
Pb15-Sn85	1.18±0.04	-0.06±0.04	0.04±0.05	0.02±0.05	21.04±0.04	22.24±0.02

In the 3D-Boltzmann plot formalism the temporal evolution of the plasma temperature can be obtained using the general expression [8]:

$$KT(t) = \frac{kT_0}{1 - kT_0 \sum_{i=1}^{S} B_i t^i} \tag{20}$$

where T_0, the plasma temperature at t=0, should be determined using conventional Boltzmann or Saha-Boltzmann plot. In our case, only the B_1 constant is important. Therefore, eq. (20) can be written as:

$$kT(t) = \frac{kT_0}{1 - kT_0 B_1 t} \tag{21}$$

To check the reliability of the above results, we have compared the predicted electron temperature calculated using these values, with the results obtained by conventional Saha-Boltzmann plot. The self-absorption effects are negligible for the ionic lines of Pb and Sn, but they should be taken into account when the neutral lines are considered, as in the Saha-Boltzmann calculations. For these lines, the effects of self-absorption were compensated using eq. (5).
Figure 3 shows the predicted temporal evolution of the plasma temperature and the results of conventional Saha-Boltzmann analysis.

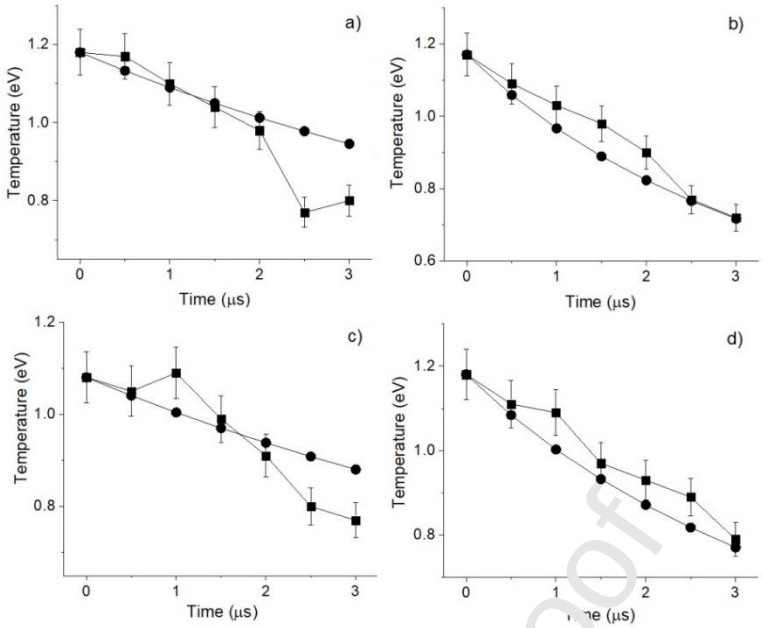

Figure 3- Comparison between the temperatures predicted by 3D-Boltzmann technique (circles) and calculated by conventional Saha-Boltzmann plot (squares). -a) 15%Pb-85%Sn, b) 30%Pb-70%Sn, c) 70%Pb-30%Sn, d) 85%Pb-15%Sn. The error bars correspond to the uncertainty in the temperature calculated using the Saha Boltzmann equation. They are due to the indeterminacy of the electronic density and the intensity of the spectral lines used in the calculation.

The predictions of eq. (21) reproduce satisfactorily the results of the conventional Saha-Boltzmann analysis (also considering the indetermination of the conventional analysis).

We should note that eq. (21) is just another way of representing the traditional Boltzmann plot when the intensities of the spectral lines used in the plot is expressed as a function of time (eq. (14)). It should also be taken into account that the use of a single constant b_1 to fit the intensities of the lines in time is justified by the short time interval analyzed (form 1 to 2.5 μs). In other circumstances and with a longer time interval, it is possible that the constants b_2 would also be needed to fit the lines and therefore there would also be two B constants (B_1 and B_2).

From the knowledge of the B_1, δ_1^{Pb}, δ_1^{Sn} and $T(t_0)$ we are now able to determine the values of q_{Sn} and q_{Pb} from eq. (13) and the corresponding concentration expressed in mass percentages of Pb and Sn from the term at right of the eq. (9). The results are shown in Table III. The concentrations reported are the average values at the four delays considered. The indetermination corresponds to the standard deviation of the results.

Table III- 3D CF-LIBS results. The indetermination corresponds to the standard deviation of the results.

	85%Pb – 15%Sn	70%Pb – 30%Sn	30%Pb – 70%Sn	15%Pb – 85%Sn
C_{Pb} (%)	87 ± 2	75 ± 2	34.8 ± 0.4	19.0 ± 0.1
C_{Sn} (%)	13 ± 2	24 ± 2	65.2 ± 0.4	81.0 ± 0.1

In table IV we show the comparison with the results of conventional Calibration-Free LIBS analysis (averaged at the different delays considered). The standard deviation of the data represents the variation of the results at different times.

Table IV- Comparison of 3D-CF-LIBS and conventional CF-LIBS. The standard deviation of the data represents the variation of the results at different times.

	Pb %		Sn %	
	3D-CF-LIBS	CF-LIBS	3D-CF-LIBS	CF-LIBS
85%Pb-15%Sn	87± 2	87 ± 3	12± 2	13 ± 3
70%Pb-30%Sn	75± 2	80± 5	24 ± 2	20 ± 4
30%Pb-70%Sn	34.8 ± 0.4	38± 7	65.2 ± 0.4	62 ± 7
15%Pb-85%Sn	19.0 ± 0.5	23± 5	81.0 ± 0.5	77± 5

The data in Table IV are shown graphically in Figures 4 and 5.

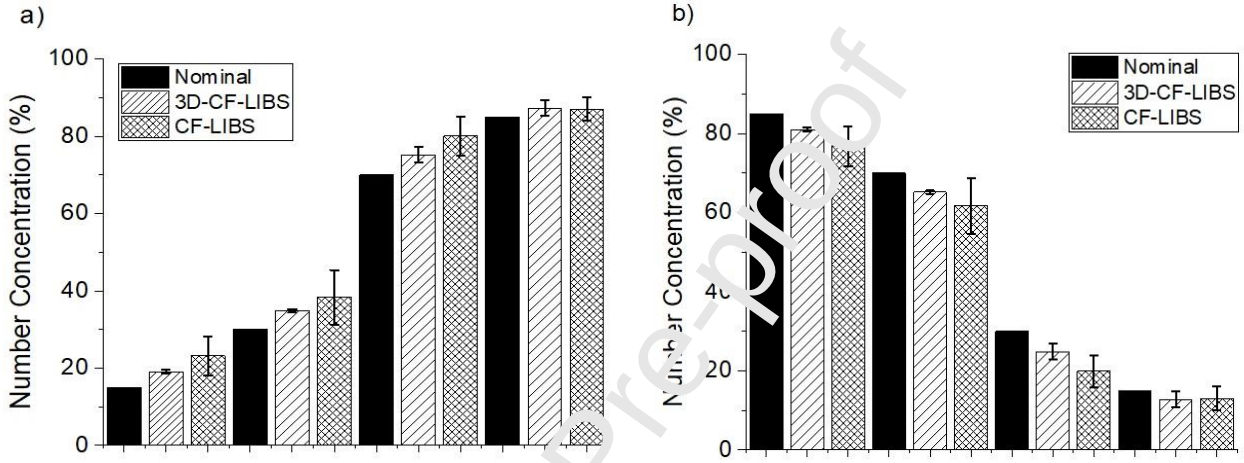

Figure 4- Comparison of the nominal stoichiometric composition of the four samples studied with the one determined by 3D-CF-LIBS and conventional CF-LIBS. a) Sn, b) Pb. The error bars correspond to the standard deviation in the calculation of the concentrations.

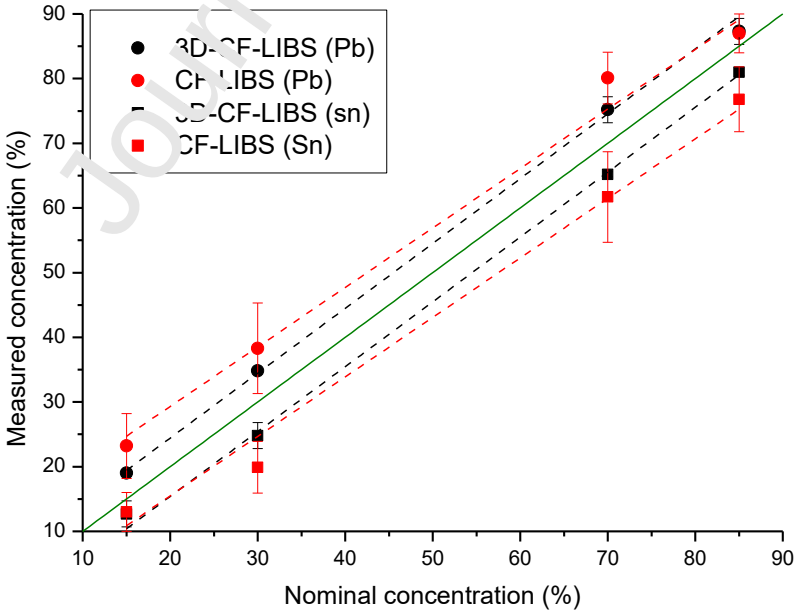

Figure 5- Comparison of the nominal stoichiometric composition of the four samples studied with the one determined by 3D-CF-LIBS (black) and conventional CF-LIBS (red). The best fitting lines of the points are dashed. The green line corresponds to the perfect correspondence between measured and nominal concentration. The error bars correspond to the standard deviation in the calculation of the concentrations.

It should be noted that both the CF-LIBS and 3D-CF-LIBS approaches overestimate the Pb concentration (probably because of the indetermination on the A_{ki} and Stark coefficients of the lines).

Table V – Comparison of the analytical results of 3D-CF-LIBS and conventional CF-LIBS

	CF-LIBS		3D-CF-LIBS	
	Pb	Sn	Pb	Sn
Slope	0.92	0.92	1.003	1.003
R^2	0.98	0.98	0.998	0.998
Intercept	10.9 %	-2.9 %	4.4 %	-4.6 %

However, as shown in Table V, the 3D-CF-LIBS method proposed in this paper is much more precise than conventional CF-LIBS. The slope of the regression plot (figure 5) for 3D-CF-LIBS is practically one, and the deviation from the nominal concentration are due to a constant bias of ± 4.5%. Also the R^2 of the regression plot is higher for 3D-CF-LIBS with respect to traditional CF-LIBS. Consider that the constant bias in a 3D-CF-LIBS could be zeroed using a One-Point-Calibration (OPC) approach [23], the improvement obtained using 3D-CF-LIBS with respect to a classical CF-LIBS approach is impressive.

The 3D-CF-LIBS method thus performs better, from an analytical point of view, with respect to conventional CF-LIBS, whose results are negatively affected by the indetermination on the electron temperature which derives by the separate analysis of the spectra acquired at different time delays. In 3D-CF-LIBS the indetermination is maintained on the value of the temperature at t=0, but the time evolution of the temperature is more precise that the one in conventional CF-LIBS, which is affected by a random indetermination passing from one spectrum to the other in the temporal sequence.

5. Conclusions

In this work we have presented a novel procedure based on the 3D Boltzmann plot method for Calibration free analysis of binary alloys. The composition of the sample is determined exploiting the temporal evolution of its spectral lines. For testing the procedure, four binary Pb - Sn alloy samples with different concentrations were used. The proposed method is much more precise than conventional CF-LIBS. The trueness of the method is within ± 5% for Pb and Sn, respectively.

Acknowledgements

The authors want to thank the CAPES (Coordenação de Aperfeiçoamento de Pessoal de nivel Superior, Brazil), the FINEP (Financiadora de Inovação e Pesquisa, Brazil), Facultad de Ciencias Exactas of the Universidad Nacional de la Plata (UNLP) for allow the PhD study to I. Urbina and the CICPBA (Comisión de Investigaciones Científicas de la Provincia de Buenos Aires) where one of the authors (FB) works as researcher.

'Appendix A. Supplementary data' and 'Supplementary data to this article can be found online at doi:...'.

References

[1] A. Ciucci, M. Corsi, V. Palleschi, S. Rastelli, A. Salvetti, E. Tognoni, New procedure for quantitative elemental analysis by laser-induced plasma spectroscopy, Appl. Spectrosc. 53 (1999) 960–964. doi:10.1366/0003702991947612.

[2] G. Cristoforetti, A. De Giacomo, M. Dell'Aglio, S. Legnaioli, E. Tognoni, V. Palleschi, N. Omenetto, Local Thermodynamic Equilibrium in Laser-Induced Breakdown Spectroscopy: Beyond the McWhirter criterion, Spectrochim. Acta - Part B At. Spectrosc. 65 (2010) 86–95. doi:10.1016/j.sab.2009.11.005.

[3] G. Amato, G. Cristoforetti, S. Legnaioli, G. Lorenzetti, V. Palleschi, F. Sorrentino, E. Tognoni, Progress towards an unassisted element identification from Laser Induced Breakdown Spectra with automatic ranking techniques inspired by text retrieval, Spectrochim. Acta - Part B At. Spectrosc. 65 (2010) 664–670. doi:10.1016/j.sab.2010.04.019.

[4] F. Rezaei, G. Cristoforetti, E. Tognoni, S. Legnaioli, V. Palleschi, A. Safi, A review of the current analytical approaches for evaluating, compensating and exploiting self-absorption in Laser Induced Breakdown Spectroscopy, Spectrochim. Acta Part B At. Spectrosc. (2020) 105878. doi:10.1016/j.sab.2020.105878.

[5] M. Corsi, G. Cristoforetti, M. Giuffrida, M. Hidalgo, S. Legnaioli, V. Palleschi, A. Salvetti, E. Tognoni, C. Vallebona, Three-dimensional analysis of laser induced plasmas in single and double pulse configuration, Spectrochim. Acta - Part B At. Spectrosc. 59 (2004) 723–735. doi:10.1016/j.sab.2004.02.001.

[6] J.A. Aguilera, C. Aragón, G. Cristoforetti, E. Tognoni, Application of calibration-free laser-induced breakdown spectroscopy to radially resolved spectra from a copper-based alloy laser-induced plasma, Spectrochim. Acta Part B At. Spectrosc. 64 (2009) 685–689. doi:10.1016/j.sab.2009.06.002.

[7] F. Bredice, F.O. Borges, H.O. Di Rocco, R.S. Mercado, M. Villagrán-Muniz, V. Palleschi, A Procedure for Estimating the Electron Temperatureand the Departure of the LTE Condition in a Time-Dependent, Spatially Homogeneous, Optically Thin Plasma, Brazilian J. Phys. 43 (2013). doi:10.1007/s13538-013-0146-x.

[8] F. Bredice, P. Pacheco Martinez, C. Sánchez-Aké, M. Villagrán-Muniz, Temporal evolution of the spectral lines emission and temperatures in laser induced plasmas through characteristic parameters, Spectrochim. Acta Part B At. Spectrosc. 107 (2015) 25–31. doi:10.1016/J.SAB.2015.02.012.

[9] F. Bredice, P. Pacheco Martinez, R. Sarmiento Mercado, C. Sánchez-Aké, M. Villagrán-Muniz, J.B. Sirven, M. El Rakwe, E. Grifoni, S. Legnaioli, G. Lorenzetti, S. Pagnotta, V. Palleschi, Determination of electron temperature temporal evolution in laser-induced plasmas through Independent Component Analysis and 3D Boltzmann plot, Spectrochim. Acta - Part B At. Spectrosc. 135 (2017). doi:10.1016/j.sab.2017.07.004.

[10] A.M. El Sherbini, T.M. El Sherbini, H. Hegazy, G. Cristoforetti, S. Legnaioli, V. Palleschi, L. Pardini, A. Salvetti, E. Tognoni, Evaluation of self-absorption coefficients of aluminum emission lines in laser-induced breakdown spectroscopy measurements, Spectrochim. Acta Part B At. Spectrosc. 60 (2005) 1573–1579. doi:10.1016/j.sab.2005.10.011.

[11] A. Alonso-Medina, C. Colon, Measured Stark Widths of Several Sn i and Sn ii Spectral

Lines in a Laser-induced Plasma , Astrophys. J. 672 (2008) 1286–1291. doi:10.1086/523844.

[12] NIST, NIST: Atomic Spectra Database Lines Form, (n.d.). https://physics.nist.gov/PhysRefData/ASD/lines_form.html (accessed April 29, 2020).

[13] A. Alonso-Medina, Transition probabilities of 30 Pb II lines of the spectrum obtained by emission of a laser-produced plasma, Phys. Scr. 55 (1997) 49–53. doi:10.1088/0031-8949/55/1/008.

[14] C. Colón, A. Alonso-Medina, Application of a laser produced plasma: Experimental Stark widths of single ionized lead lines, Spectrochim. Acta Part B At. Spectrosc. 61 (2006) 856–863. doi:10.1016/j.sab.2006.06.006.

[15] M.H. Miller, R.D. Bengtson, J.M. Lindsay, Transition probabilities and Stark-broadening parameters of neutral and singly ionized lead, Phys. Rev. A. 20 (1979) 1997–2005. doi:10.1103/PhysRevA.20.1997.

[16] C.E. Moore, Atomic Energy Levels, NIST, 1971.

[17] Atomic spectral line database from CD-ROM 23 of R. L. Kurucz., (n.d.). https://www.cfa.harvard.edu/amp/ampdata/kurucz23/sekur.html (accessed January 25, 2020).

[18] S. Djeniže, A. Srećković, Z. Nikolić, On the Sn I and Sn II Stark broadening, J. Phys. B At. Mol. Opt. Phys. 39 (2006) 3037. doi:10.1088/0953-4075/39/14/011.

[19] J. Lotrian, J. Cariou, A. Johannin-Gilles, Determination of the oscillator strengths of Sn(I) in the ultraviolet (2400-4000 Å), J. Quant. Spectrosc. Radiat. Transf. 16 (1976) 315–319. doi:10.1016/0022-4073(76)90012-1.

[20] I. Urbina, D. Carneiro, S. Rocha, E. Faria, F. Bredice, V. Palleschi, Measurement of atomic transition probabilities with laser-induced breakdown spectroscopy using the 3D Boltzmann plot method, Spectrochim. Acta Part B At. Spectrosc. 154 (2019) 91–96. doi:10.1016/j.sab.2019.02.008

[21] L. Pardini, S. Legnaioli, G. Lorenzetti, V. Palleschi, R. Gaudiuso, A. De Giacomo, D.M. Diaz Pace, F. Anabitarte Garcia, G. De Holanda Cavalcanti, C. Parigger, On the determination of plasma electron number density from Stark broadened hydrogen Balmer series lines in Laser-Induced Breakdown Spectroscopy experiments, Spectrochim. Acta - Part B At. Spectrosc. 86 (2013) 98–103. doi:10.1016/j.sab.2013.05.030.

[22] Ş. Yalçin, D.R.R. Crosley, G.P.P. Smith, G.W.W. Faris, Influence of ambient conditions on the laser air spark, Appl. Phys. B Lasers Opt. 68 (1999) 121–130. doi:10.1007/s003400050596.

[23] G.H. Cavalcanti, D.V. Teixeira, S. Legnaioli, G. Lorenzetti, L. Pardini, V. Palleschi, One-point calibration for calibration-free laser-induced breakdown spectroscopy quantitative analysis, Spectrochim. Acta - Part B At. Spectrosc. 87 (2013) 51–56. doi:10.1016/j.sab.2013.05.016.

Author Statement

Deborah Carneiro: Conceptualization, Resources, experimental data acquisition, spectral measurement.

Suellen Rocha: Conceptualization, Resources, experimental data acquisition, spectral measurement.

Eliel Farias: Conceptualization, Resources, experimental data acquisition, spectral measurement, Funding acquisition.

Ivan Urbina: Conceptualization, Methodology, formal analysis, writing, review and editing.

Fausto Bredice: Conceptualization, Methodology, formal analysis, Funding acquisition, writing, review and editing.

Vincenzo Palleschi: Conceptualization, Methodology, formal analysis, writing, review and editing.

Declaration of interests

☒ The authors declare that they have no known competing financial interests or personal relationships that could have appeared to influence the work reported in this paper.

☒ The authors declare the following financial interests/personal relationships which may be considered as potential competing interests:

The authors declare that they have no known competitive financial interests or personal relationships that may have influenced the work reported in this document.

Table I: Spectral lines used in this work.

Specie	λ (nm)	ω_s (10^{-17} nm/cm^3)	A_{kj} x10^7 (s^{-1})	g_i	E_i (cm^{-1})	g_k	E_k (cm^{-1})
Pb I	363.95	0.0153 [11]	3.2 [12]	3	7819.3	3	35287.2
Pb I	368.34	0.0131 [11]	13.7 [12]	3	7819.3	1	34959.9
Pb I	373.99	0.0112 [13]	7.3 [12]	5	21457.8	5	48188.6
Pb II	424.49	0.19 [14]	-	6	68964.3	8	92515.2
Pb II	438.65	0.13 [15]	14.71 [16]	4	68739.6	6	92530.7
Pb I	500.54	0.0075 [11]	2.7 [12]	1	29446.8	3	49439.6
Pb II	537.23	0.227 [15]	-	-	-		-
Pb II	560.89	0.14 [14]	12.45 [17]	2	59448.6	4	77272.6
Pb II	666.02	0.12 [14]	7.38 [17]	2	59448.6	2	74459.0
Sn I	380.10	0.045 [18]	3.689 [19]	5	8613.0	3	34914.3
Sn I	452.47	0.086 [11]	1.366 [19]	1	17162.5	3	39257.1
Sn II	645.35	0.29 [11]	7.0 [12]	2	56886.4	4	72377.4

Table II- Parameters of the 3D-Boltzmann plot for the samples considered. The error correspond to the standard deviation in the calculation of these coefficients

	T_0 (eV)	B_1 (μs^{-1}/eV)	δ_1^{Pb} (μs^{-1})	δ_1^{Sn} (μs^{-1})	q_{PbII}	q_{SnII}
Pb85-Sn15	1.18±0.04	-0.15±0.03	-0.8±0.3	-1.2±0.3	21.77±0.07	19.25±0.04
Pb70-Sn30	1.08±0.04	-0.07±0.02	-0.5±0.2	-0.4±0.2	22.10±0.03	20.78±0.02
Pb30-Sn70	1.17±0.04	-0.18±0.03	-0.3±0.3	-0.3±0.3	21.28±0.08	21.57±0.04
Pb15-Sn85	1.18±0.04	-0.06±0.04	0.04±0.05	0.02±0.05	21.04±0.04	22.24±0.02

Table III- 3D CF-LIBS results. The indetermination corresponds to the standard deviation of the results.

	85%Pb – 15%Sn	70%Pb – 30%Sn	30%Pb – 70%Sn	15%Pb – 85%Sn
C_{Pb} (%)	87 ± 2	75 ± 2	34.8 ± 0.4	19.0 ± 0.1
C_{Sn} (%)	13 ± 2	24 ± 2	65.2 ± 0.4	81.0 ± 0.1

Table IV- Comparison of 3D-CF-LIBS and conventional CF-LIBS. The standard deviation of the data represents the variation of the results at different times.

	Pb %		Sn %	
	3D-CF-LIBS	CF-LIBS	3D-CF-LIBS	CF-LIBS
85%Pb-15%Sn	87± 2	87 ± 3	12± 2	13 ± 3
70%Pb-30%Sn	75± 2	80± 5	24 ± 2	20 ± 4
30%Pb-70%Sn	34.8 ± 0.4	38± 7	65.2 ± 0.4	62 ± 7
15%Pb-85%Sn	19.0 ± 0.5	23± 5	81.0 ± 0.5	77± 5

Table V – Comparison of the analytical results of 3D-CF-LIBS and conventional CF-LIBS

	CF-LIBS		3D-CF-LIBS	
	Pb	Sn	Pb	Sn
Slope	0.92	0.92	1.003	1.003
R^2	0.98	0.98	0.998	0.998
Intercept	10.9 %	-2.9 %	4.4 %	-4.6 %

Highlight

*This method allows obtaining greater accuracy than the traditional Calibration Free.

*This method determines the spectral lines useful for the analysis of the plasma.

*The constants B_1 depend on the sample concentration.

*The 3D Boltzmann Plot method was applied in order to determine the temperature.